Quaternary Science Reviews 27 (2008) 1555–1570

Contents lists available at ScienceDirect

Quaternary Science Reviews

journal homepage: www.elsevier.com/locate/quascirev

Late Middle Pleistocene climate in southwestern China: inferences from the stratigraphic record of Panxian Dadong Cave, Guizhou

Panagiotis Karkanas [a,*], Lynne A. Schepartz [b], Sari Miller-Antonio [c], Wang Wei [d], Huang Weiwen [e]

[a] Ephoreia of Palaeoanthropology–Speleology of Southern Greece, Ardittou 34b, 11636 Athens, Greece
[b] Department of Anthropology, Florida State University, 1847 West Tennessee Street, Tallahassee, FL 32306, USA
[c] Department of Anthropology/Geography, California State University, Stanislaus, One University Circle, Turlock, CA 95382, USA
[d] Natural History Museum of Guangxi, No. 1-1 East Renmin Road, Nanning 530012, China
[e] Institute of Vertebrate Paleontology and Paleoanthropology, P.O. Box 643, Beijing, China

ARTICLE INFO

Article history:
Received 8 February 2008
Received in revised form
13 May 2008
Accepted 21 May 2008

ABSTRACT

Panxian Dadong Cave, situated in the subtropical zone of southwestern China, preserves a fan-like sedimentary sequence close to its entrance that spans the period between MIS 8 and 5 (300–130 ka). The frequent alternation of flowstone formation, cementation, clastic deposition, and frost activity in the depositional sequence makes it ideal for reconstructing the environmental conditions prevailing during the later Middle Pleistocene on the Guizhou Plateau.

Macroscopic and microscopic sedimentary analyses determine that clastic deposits were entering the cave in the form of intermittent cohesive debris flows and sheetflows during cold and relatively dry climatic conditions when vegetation cover was reduced. Interlayered impure flowstones were forming during wetter phases but still under glacial conditions. Seasonally freezing temperatures are deduced from the frequent occurrence of cycles of well-developed freeze–thaw features affecting both the clastic parts of the sequence and the flowstones as they were deposited. The described depositional processes were responsible for lateral redistribution on the fan surface of bone remains and lithic artifacts that were accumulating on the surface as a result of hominid activities. During the intervening interglacial stages (MIS 7 and possibly MIS 5) clastic deposition was considerably reduced and only thin flowstone caps and weathering manganese–iron crusts were forming. It is suggested that precipitation was much higher during glacial intervals than interglacials under a predominantly cold climate. Dadong Cave provides a good example of very cold and wet climatic conditions during glacials in the subtropics of East Asia.

1. Introduction

Caves can act as perfect sedimentary traps as they are protected from many post-depositional subaerial processes, and their sedimentary facies have been used to interpret and reconstruct depositional histories that can track changes in earth system processes (Springer, 2005). These data also yield insights into the climate and landscape evolution of the area. Speleothems, in particular, are regarded as appropriate terrestrial analogs to the deep sea and ice cores used in establishing a detailed terrestrial climatic record (Bar-Matthews et al., 2003). Conversely, clastic cave sediments have been more rarely used to infer climatic signals. In most cases they are considered to be coarse proxies of environmental changes. Many variables affect the formation of clastic sediments, therefore the paleoclimatic significance of these deposits is complex and open to interpretation (for a review see Farrand, 2001; Woodward and Goldberg, 2001). However, there are certain cave sedimentary features like cryogenic features that are useful climatic proxies, and when their study is combined with stratigraphic and field sedimentary facies analysis, these features can provide important clues to the climatic and geomorphological evolution of an area. Petrographic or micromorphological studies of cave sediments are particularly useful for revealing features related to frost activity and ice segregation (Gremaschi and Van Vliet-Lanoë, 1990; Courty and Vallverdu, 2001; Karkanas, 2001). In addition, the study of sedimentary facies at the microscopic level provides additional information on the depositional processes (Knapp et al., 2004). The microscopic approach to studying cave sediments has a wide application in caves with archaeological remains (Goldberg and Sherwood,

* Corresponding author. Tel.: +30 21 07 56 14 11; fax: +30 21 07 56 14 38.
E-mail addresses: pkarkanas@hua.gr (P. Karkanas), lschepartz@fsu.edu (L.A. Schepartz), smillerantonio@csustan.edu (S. Miller-Antonio), wangwei12841@163.com (W. Wang), huangweiwen@ivpp.ac.cn (W. Huang).

0277-3791/$ - see front matter © 2008 Elsevier Ltd. All rights reserved.
doi:10.1016/j.quascirev.2008.05.005

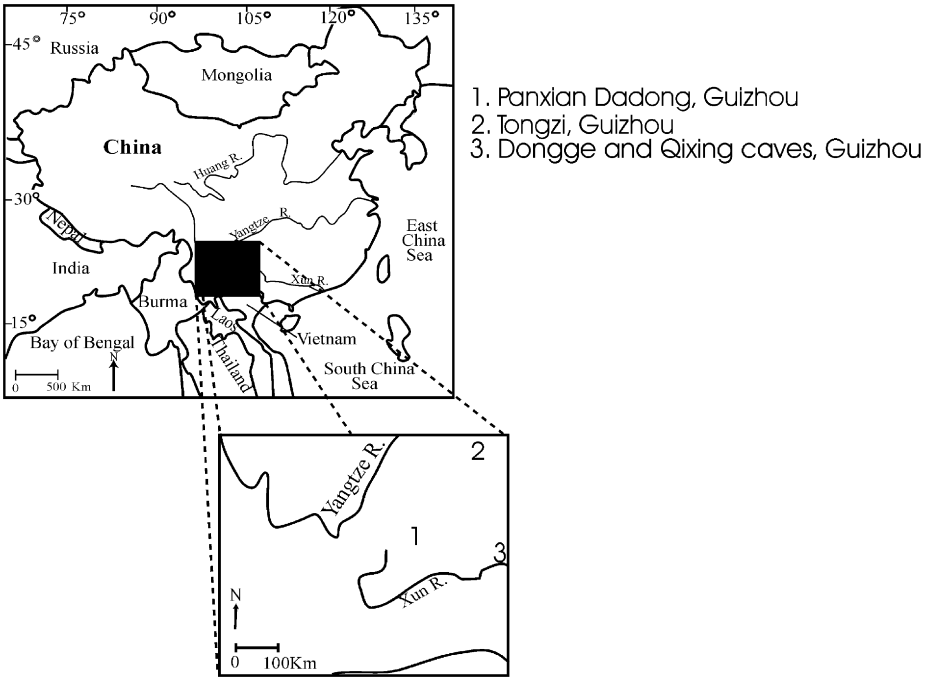

Fig. 1. Map of China with the location of Dadong Cave (1) relative to Tongzi Cave (2) and the Dongge and Qixing caves (3).

2006). Data from cave sediments provide contextual information for the interpretation of archaeological remains and the human role in formation of the deposits (Courty et al., 1989).

This study is concerned with a site located in an area with meager climatic information, but the region is of major importance in understanding monsoon changes related to glacial and interglacial stages. Panxian Dadong Cave lies in the western part of the Guizhou Plateau that is part of the southeastern extension of the Tibetan Plateau (Fig. 1). A preliminary study documented that the cave deposits have a rich record of cyclical climatic changes (Wang et al., 2004). Paleoclimate studies have been conducted in central China using loess sequences (Kukla, 1987) and on the Qinghai-Xizang (Tibetan) Plateau using lake and ice-core records (Lister et al., 1991; Thompson et al., 1997), but few paleoclimate records exist from southwestern subtropical China. The majority of them are from the Holocene and the late Pleistocene (Zheng et al., 2002; Yuan et al., 2004; Zhang et al., 2004; Zhu et al., 2006). Therefore, our aim is to present a combined microscopic and macroscopic sedimentary facies analysis of a cave sequence within an established chronological framework to infer climatic changes between ca 300–130 ka. As these cave sediments also contain archaeological remains these data can also be used to establish the implications for the human use of the cave, and fill a critical gap in the climate record during the time when humans were broadly dispersed across the East Asian landscape.

2. Cave setting and environment

2.1. Cave formation

The Guizhou Plateau where Panxian Dadong Cave is located (25°37′38″N, 104°44′E) is composed of Carboniferous and Permian limestones, basalt, shale, sandstone, and coal formations. The general elevation ranges between 1400 and 2000 m. Dadong is the middle cave in a series of interconnecting karstic caverns within a 230 m hill. The hill itself is situated in a small karstic valley (polje) that lies at an elevation of 1630 m above sea level. The eastern facing cave entrance is 55 m wide and 50 m high and located 32 m above the valley floor (Fig. 2). The main chamber narrows slightly to become an average 35 m wide and 30 m high phreatic passage that runs over 220 m in length and covers an area of over 8000 m^2. The area is a typical karst combination of peak clusters and depressions (Fig. 2). The cave itself is a sinkhole formation, the result of neotectonic uplift, where underground rivers with phreatic features drained through (Xiong and Liu, 1997). The cave walls bear large asymmetrical meter-sized scallops showing a direction of flow towards the interior of the cave and evident of a period when the cave was an active sinkhole. The continuous uplift of the cave and lowering of the base level rendered the Dadong passage dry. After that, clastic sedimentation alternating with flowstone formations prevailed in the cave. A more recent collapse at the back of the cave has produced a pitfall connecting the cave with the top of the hill.

The entrance of the cave is dominated by a huge complex columnar speleothem from which an extensive flowstone formation spreads and covers the present floor of the cave (Figs. 3–5). Several other flowstone formations intercalated within the studied clastic deposits also spread down from the modern entrance along the northern wall and the area of the columnar speleothem, forming a gently sloping fan towards the interior of the cave.

2.2. Climatic data

The vegetation of the Dadong area is characterized by mixed evergreen coniferous, broad leaf, and deciduous forest. Mean annual temperature is about 14 °C and mean annual precipitation is approximately 1400 mm. In summer, the monthly highest mean temperature is observed during July (20–21 °C) and in winter the lowest is in January (4–5 °C). The climate is subtropical (humid in summer and dry in spring). From mid-May through the beginning of October the area is influenced by summer monsoons. Toward the end of fall and into winter, cold air from the north and warm air from the south meet in this area forming a stationary front and

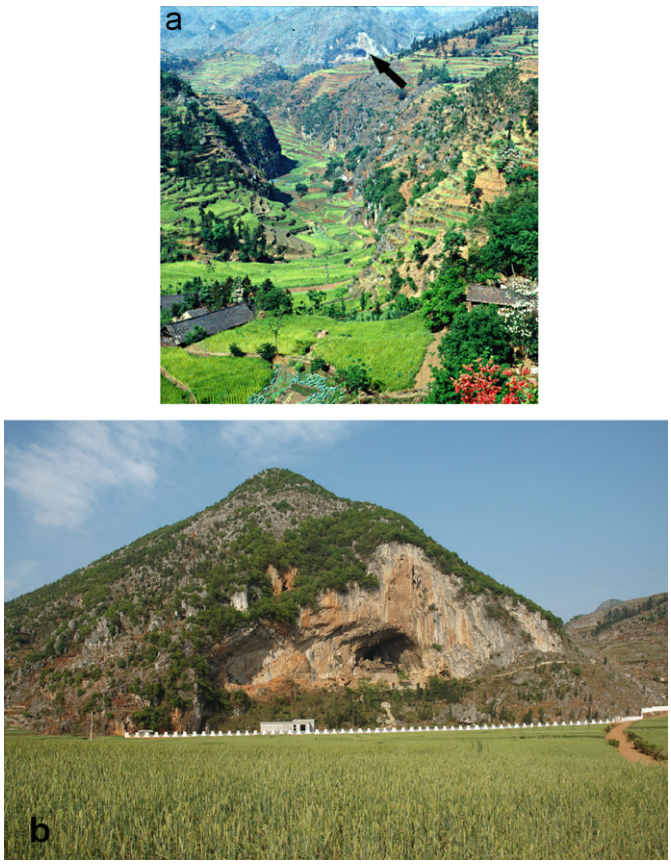

Fig. 2. (a) Photograph of the area around Dadong Cave (with arrow) showing the ragged karstic topography. Note the peak clusters on the very upper left edge of the photograph. (b) The entrance of the cave in the hill above the karstic valley in front.

establishing a regime of rainy weather. From February to early May, the weather is very dry as a result of strong south-west winds. In summary, precipitation during the summer season is mainly controlled by the East Asian summer monsoon, while the meteoric precipitation in the winter season is mainly controlled by the cold fronts of the winter monsoon and the southwest warm-wet air masses (Zhang et al., 2004).

2.3. Archaeology

Panxian Dadong contains an extensive record of human activities during the late Middle Pleistocene. Stone tools of limestone, basalt, and chert were recovered from the cave excavation and there is some evidence that *Rhinoceros sinensis* teeth were also flaked to produce small scrapers (Miller-Antonio et al., 2000, 2004). The stone tools are associated with a rich assemblage of the Middle Pleistocene southern Chinese *Ailuropoda–Stegodon* fauna predominated by *R. sinensis* and *Stegodon orientalis* elements (Schepartz et al., 2003; Bekken et al., 2004). Other taxa include a variety of ungulates (cervids, bovids, rhinoceroses, pigs, giant tapirs, muntjak, and musk deer), insectivores, rodents (white-toothed shrew, porcupine, and bamboo rat), and small numbers of carnivores (tiger, bear, hyena, weasel, and tiger cat) and primates such as macaques. The excavation also yielded five *Homo sapiens* teeth. Bones and artifacts show very little indication of transport or subaerial weathering so it is inferred that they were accumulating inside the cave. The exact process of accumulation is thus of primary interest for reconstructing the human use of the cave and exploitation of faunal resources in the area.

3. Methods

The recent excavated part of the sedimentary sequence is approximately 5 m deep. It runs from the northern wall to the center of the cave at roughly the middle of the main chamber (Fig. 3). Material was removed horizontally with artifacts and bones larger than 2.5 cm piece-plotted with a total station as they were uncovered and smaller material recovered with screening and hand sorting.

In addition to field stratigraphic and sedimentological observations, 28 intact blocks of sediment were collected from the profiles of the excavation for micromorphological and petrographic study. Their locations are shown in Fig. 5. Strongly cemented sediments were removed by cutting blocks of appropriate dimensions (ca $(10–30)\times 10\times 10$ cm) using an angle grinder, while loose samples were first jacketed with plaster of Paris to secure undisturbed samples. All samples were impregnated with polyester resin under vacuum. In total 34 medium (3×5 cm) and 28 large format (5×7 cm) thin sections were produced. They were studied under a stereomicroscope at magnifications of 5–40× and a polarizing microscope at magnifications ranging from 15× to 400×. Micromorphological description follows the terminology of Bullock et al. (1985) as modified by Stoops (2003), whereas certain features related to calcite cementation were described according to the standard petrographic terminology of carbonate rocks (Scholle and Ulmer-Scholle, 2003).

The mineralogy of selective bulk samples was analyzed with Fourier Transform Infrared Spectroscopy (FTIR) in an attempt to decipher the mineralogical features identified in the thin sections. About 0.5 mg of sediment was mixed with about 4 mg of KBr and hand-pressed to produce a pellet that was introduced into the chamber of a MIDAC Corporation (Costa Mesa, CA) infrared spectrometer. Spectra were obtained at 4 cm^{-1} resolution and interpreted using a built-in library (for more details, see Weiner et al., 1993).

4. Stratigraphy

The deposits of the main chamber make a gently inclined slope from the entrance. Some key stratigraphic markers can be roughly followed in their full extension in the 1996–2005 excavation (the area where detailed observation and analysis of the deposits was conducted) as well as in the previous excavated trenches (see Figs. 4 and 5). Therefore, continuity of strata can be determined and reworking from the underlying layers (e.g. undermined flowstones) is not observed—rendering the sequence reliable for environmental interpretation (cf Moriarty et al., 2000).

A first generation of a series of complex speleothem formations (bell canopies, after Hill and Forti, 1997) on the side walls of the main cave passage is one of the earliest sedimentary phases that is now partially buried by the clastic sedimentary sequence (Fig. 4). These speleothems grew below a line representing a former water level inside the cave at approximately 4.5 m above the present floor. Below this line the walls are smoothly corroded overprinting the scallop formations. The water-line corresponds to a period when the entrance of the cave was close to the base of the valley and the Dadong passage was seasonally flooded (Xiong and Liu, 1997). The canopies overprint the water-marks and thus have been formed after the cave was abandoned by stream processes, the passage was drained, and clastic sediment started entering from the modern entrance. The sedimentary sequence is inclined to the back of the cave, and from the northern wall to the center.

The sedimentary sequence comprises clastic sediments with thin intercalating capping flowstones and a top thick flowstone. In

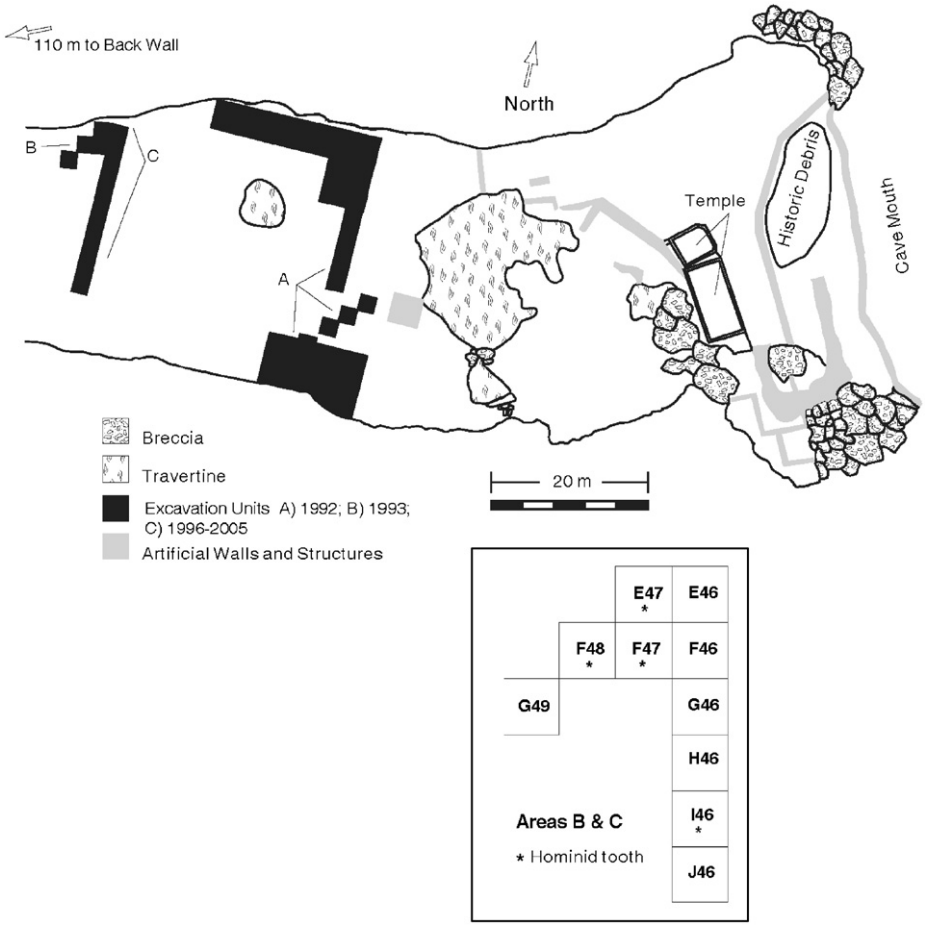

Fig. 3. Panxian Dadong main chamber excavations. The excavation area designated as Area C consists of a long trench that was cleared of approximately one meter of disturbed sediments. Controlled excavations then followed in the north portion of the trench, as shown in the inset.

the lower parts, the clastic sediments are mainly massive silts changing to alternating bedded gravels, clay-rich deposits, and boulder lags. Field and microscopic observations of the individual strata of the cave are described in Table 1 and stratigraphic sections are shown in Figs. 5 and 6.

5. Interpretation of depositional facies and post-depositional alterations

The great potential for reconstructing the environmental conditions in Dadong warrants a fuller interpretation of the depositional features. Although the actual sedimentary type may not necessarily be diagnostic of surface environmental conditions—because of large delays between surface processes and final sedimentation in caves—the processes responsible for the final deposition are directly linked with surface processes (Moriarty et al., 2000). The Dadong deposits form a small low angle fan that is directly connected to the entrance and the outside environment. Thus, the main source of sediment input is well defined. Furthermore, the sequencing of flowstones versus clastic deposition is suggested to be excellent for reconstructing environmental conditions in caves (Moriarty et al., 2000). Capping flowstones preserve the integrity of the stratigraphy and prevent post-depositional mixing and slumping. There are also several other criteria that, in the case of Dadong, can constrain the interpretation of the sediment, such as freeze–thaw features that show a very well-developed cyclical pattern. In this respect, depositional facies and their post-depositional evolution can be used to deduce paleoenvironments. The main depositional facies and post-depositional alterations (a total of six), as well as their environmental significance, are as follows.

5.1. Massive silty calcite facies

The lower part of the clastic sequence, i.e. layers XII–VIII, is characterized by massive moderately to well-sorted silty calcitic sediment with some dispersed rounded calcareous clasts and few soil lumps (Figs. 5 and 6; Table 1). Their massive appearance is probably due to deposition from flash flood episodes or hyperconcentrating flows dumping loess-like material from the valley inside the cave. Although loess is not reported from this area, the large amount of clastic silt sized calcite can be considered to be typical dust sediment (Nickling, 1994) of mostly local origin (limestone plateau). It is evident, however, that the sediment is actually redeposited loess-soil as it has a moderate content of clay and clay soil lumps. A temporarily elevated water table is also suggested by the presence of organo-metallic impregnative and iron–manganese aggregate nodules (Table 1).

5.2. Alternation of bedded gravel, matrix-rich facies, and boulder lags

Layers VII and VI and above mark a change to a different sedimentation pattern characterized by alternating clast- to matrix-supported gravel and matrix-rich beds (Figs. 5–8;

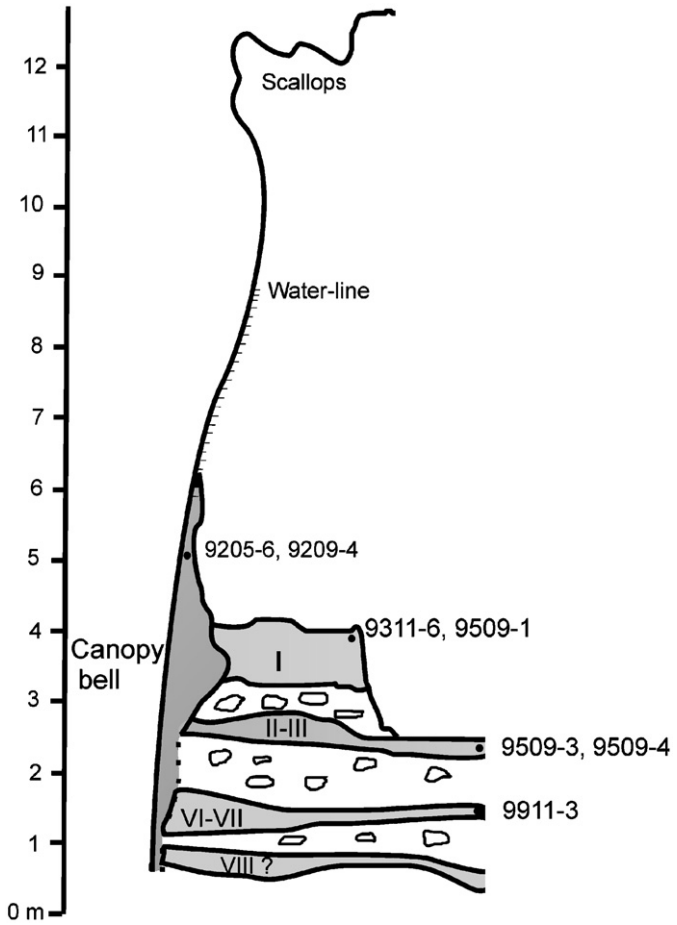

Fig. 4. Sketch section showing relationships between the canopy bell, water-line, and dated speleothems (see also Table 2). Stratigraphy of flowstones is based on observations in the old excavated Area A, northern wall.

Table 1). Their field and microscopic features suggest deposition from episodic sediment gravity flows and water flows forming a small fan-like feature from the present entrance to the center of the main chamber. Sediment gravity flows are mainly in the form of cohesive debris flows characterized by matrix to clast-supported tabular beds with floating boulders, coarse "tails", and imbrication of coarser particles (cf Blikra and Nemec, 1998). They were formed when colluvium that had accumulated in the entrance was destabilized by water saturation and failed under the force of gravity. It was transformed into a high viscosity flow that fanned down into the main chamber. Water flows are restricted to sheetflows forming tabular beds of plane-parallel stratified subrounded gravels (cf Blikra and Nemec, 1998). They were formed by shallow unconfined (not channelized) water flow washing the fan. Sediment feeding was from the modern entrance and close to the northern wall as suggested by the general geometry of the sequence, the lateral grading of the individual layers, and the cementation pattern; all have a source from the northern cave wall and the entrance.

What is of major interest is the content of reworked calcareous clastic material with compound pisoid structure derived from already deposited and cemented material inside the cave (Fig. 9). These features are mostly associated with gravelly beds or impure (clastic-rich) flowstone formations. In contrast, the clayey matrix-rich beds normally do not contain complex pisoids, but instead are enriched in decayed organic matter and concentric aggregate organo-metallic nodules.

The formation of this alternation of clastic sediment requires an open entrance that permits unconfined water flow down the opening. These are regularly associated with frost action (see below) and may derive from surges of sediment-laden water related to snow melt during a predominantly cold climate with reduced vegetation cover. Some of the thicker matrix-rich beds might have been formed during a milder climatic regime given their high organic content and reduced intensity of freeze–thaw features.

5.3. Flowstones

Since all flowstones in Dadong Cave are contaminated with clastic material, an open entrance is hypothesized permitting episodic sediment and water flow (cf Moriarty et al., 2000). Flowstone formation requires relatively continuous precipitation of calcite from water films flowing over the surface, and they have been interpreted as indicators of former warmer and wetter climates in temperate zones or increased precipitation in arid desert settings (e.g. Baker et al., 1993; Ayliffe et al., 1998). In the case of Dadong, extensive flowstone formations are related to cold and wet environmental conditions, as they are closely associated with intensive freeze–thaw activity (see below). In particular, layer I is an impressive thick impure flowstone (Figs. 4–6 and 10) covering much of the present surface of the cave and containing abundant evidence of ongoing frost action. The same activity, but less extensively, can be seen in the impure flowstones of layers VI, IV and II (Fig. 5). However, some thin massive impure flowstone formations without evidence of freeze–thaw activity are related with the crust formations found in layer VII and probably layer VIa (Fig. 7) as well as in the capping crust of layer I. These were presumably deposited during relatively wet but warmer periods.

5.4. Calcite cementation

In Dadong cave calcite cementation of clastic layers is in the form of phreatic and vadose calcite precipitation inside the pores of the sediment (Figs. 11b and 12). Formation of bladed rims of calcite and complete filling of the pores with blocky sparite (layers XII, XI, IX, VIII, III, II and I: Table 1) requires a continuous immersion of the sediment in water (Scholle and Ulmer-Scholle, 2003). It is most likely that occasionally the cave floor was saturated by water with water-filled pools occupying the surface. Cementation is always related with intensive frost action but usually it post-dates it.

5.5. Frost action

Most of the layers in Dadong Cave are characterized by fissure to incipient platy microstructures (Figs. 11a and 13) that in most cases give way upwards to lenticular and finally granular microstructures (Figs. 11, 12 and 14–17; Table 1). In several cases laminated silty calcite link cappings support several granules (Figs. 11 and 12) and loose sorted grains fill the voids (Fig. 16). These types of microstructures are typical of frost activity and are reproducible by experiments (Van Vliet-Lanoë et al., 1984; Gremaschi and Van Vliet-Lanoë, 1990). It is well known that in seasonally frozen soils when soil water is transformed into ice the latter is crystallized outside the groundmass and takes the form of ice lenses that are parallel to the soil surface. The stresses thus produced bring about fragmentation and the production of incipient fissures that with repeating freezing give way to platy and lenticular aggregates known also as ice lensing. Further fragmentation produces fine particles that are transported by the

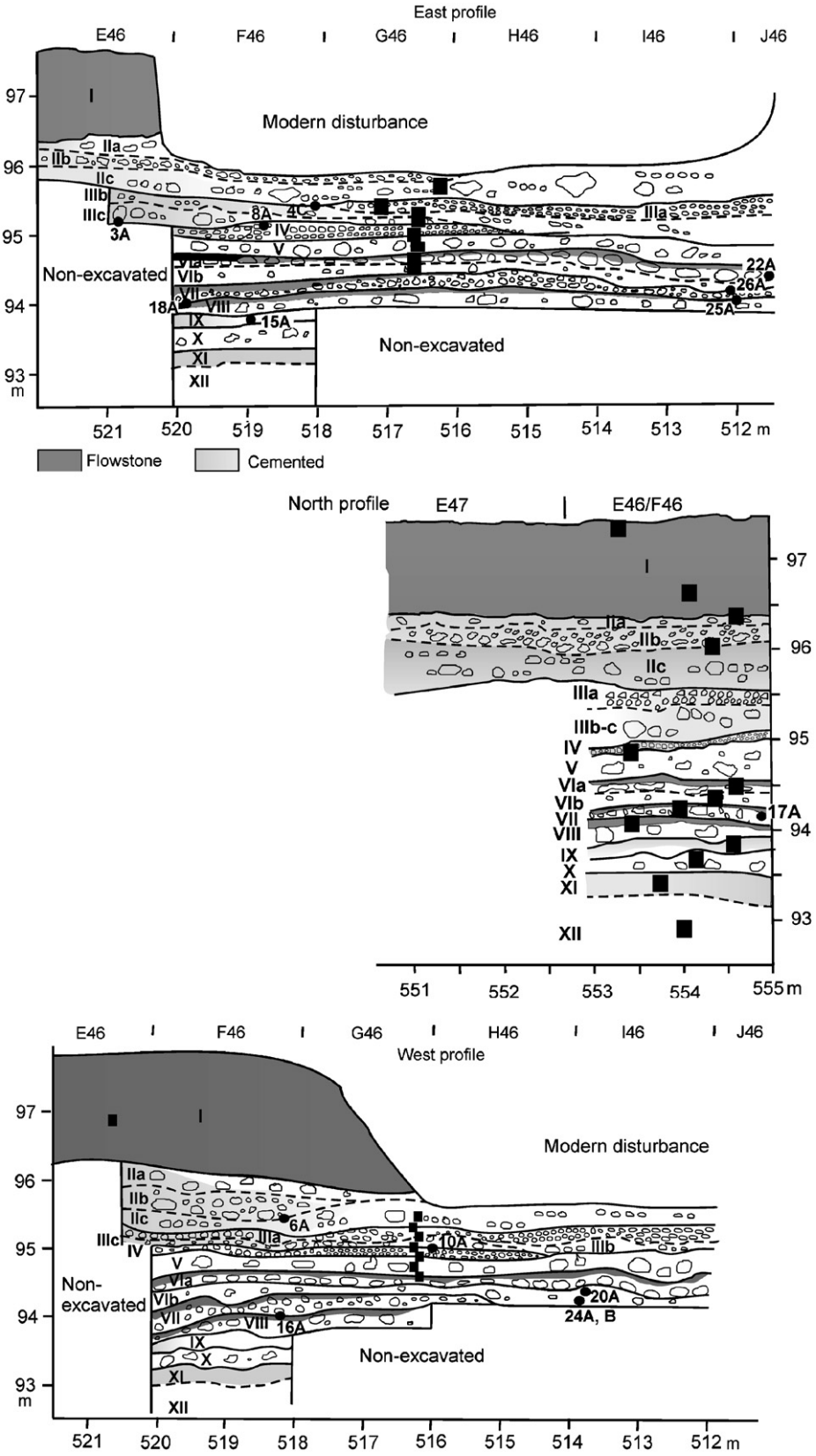

Fig. 5. Stratigraphic sections of excavated area C (refer to Fig. 3) showing the location of the micromorphological samples (black rectangles; not to scale) and the location of the dated fossil teeth (black dots with Arabic numbers: see Table 3).

melt water and accumulate as cappings on the upper part of the aggregates (Courty et al., 1989, pp. 160–163). In particular the complex granular structure observed in Dadong Cave sediments enclosing several generations of pisoids (Figs. 14b and 9) is attributed to gelifluction, resulting from an increasing slope or water flow (Van Vliet-Lanoë et al., 1984).

Table 1
Description of the stratigraphy of the Dadong Cave sedimentary sequence, including macroscopic and microscopic observations

Layer	Thickness (cm)	Field observations	Micromorphological observations
XII	50–60	A thick massive yellowish brown and slightly cemented sediment with very few floating pebbles.	Under the microscope it has a sorted fine silty, mostly calcitic texture with a few dispersed clay lumps. Very few fine silty quartz grains were also identified. Organo-metallic impregnated and iron–manganese aggregate nodules are widespread. A few very well-rounded to subrounded calcareous aggregates with organic hypocoatings are visible. The microstructure is fissure to incipient platy structure (Fig. 11a). Very few voids show isopachous rims or complete filling of equant sparite.
XI	30	The same sediment as XII but moderately cemented.	Stronger development of lenticular and granular microstructures (Fig. 11b) and some clastic-rich calcite cappings. Most of the pores have isopachous rims or are sealed with sparitic calcite of phreatic origin (Fig. 11b). However, vadose laminated silty clay coatings in the form of pendants are also observed (Fig. 11b). Secondary micritization is evident in the upper part.
X	20	A massive yellowish brown layer with very few floating rounded limestone fragments ranging up to boulder size. The layer thins out towards the center of the cave.	Moderate unsorted sandy silt calcitic sediment with some rounded calcareous aggregates, limestone and speleothem fragments. Some of the aggregates and fragments have organic and organo-metallic hypocoatings. There are several cases where the clastic-rich calcareous aggregates have an incipient pisoid structure (concentric nucleic to aggregate nodules). The matrix also has organo-metallic impregnated and iron–manganese aggregate nodules. Fissure and incipient platy microstructure is evident towards the upper part. A few silty clay coatings were also identified.
IX	30	A massive reddish yellow to brownish locally cemented layer.	A well-sorted calcitic silt with some clay and moderately developed organo-metallic impregnated and iron–manganese aggregate nodules. Some impure calcareous aggregates with pisoid structure and few rounded limestone and speleothem fragments were identified. Well-developed lenticular microstructure (Fig. 14a) that grades upwards into a granular one. A few silty calcite cappings and some laminated dusty clay coatings are observed. Most of the pores are lined with phreatic bladed calcite with some of them completely sealed.
VIII	10–20	An unconsolidated reddish brown fine-grained layer with subrounded limestone boulders floated in the matrix. A thin calcareous surface crust separates layer VIII from the overlying layer VII. Bones and lithic artifacts are widespread (prior to this layer, there was little bone recovered and few lithic artifacts).	The matrix is more unsorted than that of the layer below as evidenced by the presence of some angular sandy grains. The microstructure is lenticular that upwards grades to granular. Laminated silty calcite link cappings support several grains (Fig. 14b). Impure calcareous aggregates with pisoid structures are regularly observed. Indeed, the characteristic of this layer is a complex granular structure enclosing several generations of pisoids (Fig. 14b). Thick laminated reddish dusty clay coatings are seen everywhere. Organo-metallic hypocoating is widespread on the aggregates. Towards the top there is phreatic calcite cementation in the form of isopachous bladed calcite and infills of sparitic calcite. A calcitic crust is developed on top of the granular microstructure enclosing some of the granules within it. The crust is characterized by compound clay and iron–manganese impregnative features (Fig. 18).
VII	10–30	A matrix-supported gravel with sizes ranging up to boulders. The gravel is subangular to subrounded. Close to the northern wall a flowstone cap is evident.	Some of the finer clastic sediment in between the boulders displays granular microstructure and complex pisoid structures. However, the flowstone cap has a massive microstructure.
VI	30–40	VIb: A brownish lenticular fine-grained bed. Some gravel is dispersed inside with subrounded forms. It also contains a dense accumulation of bone and lithic artifacts. VIa: A boulder lag with a thin flowstone cap on top (Fig. 7). It contains a dense accumulation of bone and lithic artifacts.	Lenticular and granular microstructures are widespread. Complex redeposited pisoid structures are often encountered. Locally, both the matrix and the flowstone are characterized by lenticular to granular microstructure.
V	40–50	A brownish fine-grained deposit with floating boulders and fine gravel (Fig. 7). Bone and lithic artifacts are less abundant.	An unsorted clayey loam containing many organo-metallic impregnative nodules, some of them with concentric and dendritic structures. Remnants of decayed organic matter are abundant. From the top to the bottom the microstructure changes from lenticular, to platy and fissure, and finally to massive (Figs. 15 and 16).
IV	10–20	A tabular bed of mostly clast-supported subrounded to rounded gravel that is moderately sorted and plane-parallel stratified (Fig. 7). It thins out from the northern wall to the center of the cave. It is also strongly cemented close to the wall giving way to impure thin flowstone. Contains bones and lithic artifacts.	The fine matrix in between the gravel is characterized by erratic development of lenticular microstructures and a compound pisoid granular structure. In some areas the lenticular microstructure continues undisturbed in the underlying layer V.

Table 1 (*continued*)

Layer	Thickness (cm)	Field observations	Micromorphological observations
III (IIIa–c)	50–70	IIIb–IIIc: Matrix-rich tabular beds that are more boulder-rich in the north and become more fine-grained in the south. They contain floating cobbles and boulders with occasionally clast-supported 'tails' and crude imbrication (Fig. 7). Cementation is locally intense towards the northern profile where bouldery and gravelly facies give way to flowstone formations (Fig. 5).	Reddish brown loam with microscopic organo-metallic nodules and remnants of decayed organic matter. Platy and lenticular microstructures are well-developed.
		IIIa: A tabular bed with clast- to matrix-supported gravel. The gravel is subrounded and shows crude plane-parallel stratification and weakly erosional contacts with the underlying layer (Fig. 8). This layer also yields a relatively dense concentration of fauna as well as lithic artifacts with a conspicuously high proportion of teeth towards its base (Schepartz et al., 2003).	Several phases of alternating platy, lenticular and granular microstructures are observed. Widespread development of complex pisoid structures. Thin impure flowstone formations also show lenticular microstructures.
II (IIa–c)	100	IIc: A dark brown clayey bed that contains floating boulders and finer gravel arranged in clusters and lines. It also becomes cemented towards the northern wall. Fragmentary bone and lithic artifacts are abundant.	Alternating sorted and unsorted loamy increments. A high amount of decayed organic matter and organo-metallic nodules are observed (Fig. 16). It is characterized by well-developed fissure to incipient platy microstructure (Fig. 16).
		IIa–IIb: A sequence of gravelly tabular beds that become cemented towards the northern wall. Layer IIb has a bouldery base and show local crude stratification. It also thin out towards the center of the cave.	The loamy matrix shows lenticular microstructure.
I	150	A thick laminated clastic-rich flowstone formation (Figs. 6 and 10). Locally, in between the calcareous laminae, there are thin uncemented reddish clayey laminae. Bones and artifacts occur in very high concentration.	Redeposited clastic material in the form of composite calcareous pisoid structures (Fig. 9) that are welded in well- developed lenticular and granular microstructures with calcitic link cappings (Fig. 12). The structures are arranged in increments, with each one starting with coarse lenticular microstructure giving way to fine lenticular and finally typically capped by a laminated clastic-rich calcite crust (Fig. 17). On the crust fine crystal fans, consisting of radial calcite, are occasionally developed. Each increment is cemented with sparitic calcite filling the interaggregate fissures (Fig. 12). On the contact with the underlying increment vadose calcite coatings (pendants) are overlain by dusty clay coatings.
			The top ca 10 cm is characterized by mesoscopic fenestral porosity and microscopic vesicles.

In the Dadong Cave sequence discrete frost events can be recognized, as they are separated by cementation events not affected by frost action or showing repeated cycles with increasing intensity upwards from angular fissuring to planar, lenticular and finally granular microstructures (Fig. 15). Freeze–thaw features are observed both in fine-grained and gravelly layers. However, some thick clayey layers do not show well-developed features but only fissuring and incipient coarse platy microstructure (Fig. 13). This is probably due to a combination of high sedimentation rate and low intensity of frost action. It is also clear that some of these layers were affected after being deposited, whereas others were affected during their formation. Nevertheless, on the basis of their recurring pattern and spatial development, it appears that almost all sedimentary layers more or less were affected by freeze–thaw activity during or shortly after their formation. The only exception seems to be the crust horizons in layers VI and VII and the capping surface of layer I. It is also important to stress that ice lensing requires that the sediment contains some water in order for ice to form.

5.6. Weathered crusts

The weathered crusts found in layers VI and VII (Table 1) represent depositional hiatuses. They are characterized by weathering iron–manganese rinds on boulder lags and complex iron–manganese impregnative crust pedofeatures overprinting impure flowstone formations (Figs. 7 and 18). The paucity of clastic input implies stabilization of the soil on the hills above the cave and thus the existence of a tree cover under probable humid warm climatic conditions. However, under such conditions extensive speleothem formations are expected—something not observed in Dadong.

6. Chronological framework and summary of sedimentary history

The regular interlaminated clastic sediment, impure flowstones, phreatic and vadose cementation, and frost activity in Dadong is related to a cold environment with fluctuating humidity but a predominantly wet climatic regime. Major episodes of uncemented clastic sedimentation are probably related to reduced humidity and limited vegetation cover, whereas calcite cementation and flowstone formation are related to wetter phases. The exceptions to this picture are probably the weathered crust–flowstone couplets that should imply more stable periods with reduced erosion and extensive vegetation cover.

Absolute age estimates for the sedimentary deposits of Dadong Cave include U-series ages from speleothems (Table 2; Fig. 4)

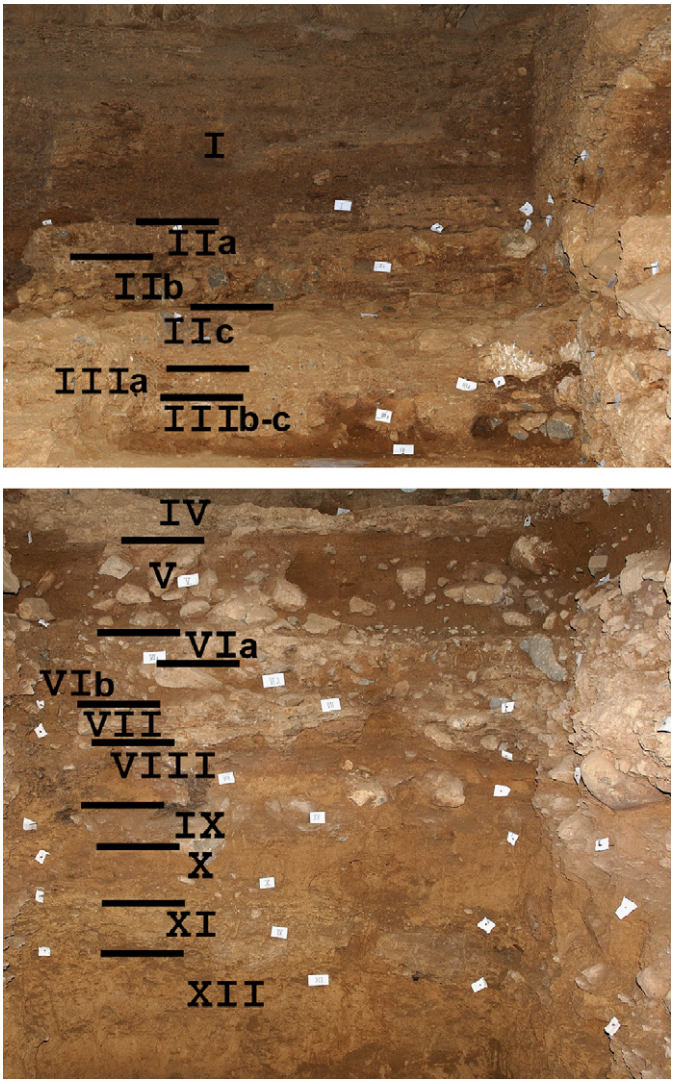

Fig. 6. General stratigraphy of the northern excavation profile. Note the fine-grained nature of the lower part, the boulder- and gravel-rich middle part and the flowstone formations of the upper part. The height is 5 m.

Fig. 7. Part of the stratigraphy of the eastern excavation profile. Note the crust on top of layer VIa (with arrow), the floating boulders in layer V, and the coarse tails and imbrication in layers IIIb and c. Height of photo is 1.5 m.

Fig. 8. Detail of layer III1 (between horizontal bars) with planar stratified gravel and weakly erosional lower contact.

(Shen et al., 1997) and coupled ESR/uranium series ages for fossil teeth (Table 3; Fig. 5) (Jones et al., 2004). Although both methods produced a wide spread of ages, in general they are comparable and the ages are in relatively good stratigraphic order. Some minor discrepancies observed in the lower group of the coupled ESR/uranium series ages (Table 3) can be explained by depositional processes (see below). In the present work, we use the above age estimates to produce a general chronological framework for groups of layers and thus the resolution offered by the available dating results is satisfactory. In addition, the observed frost action puts further constraints on the age determination.

Preliminary U-Th dates obtained from two of the oldest speleothem formations (bell canopies) on the cave walls that are buried inside the clastic sequence are greater than 300 ka and probably averaged to about 330 ka (Fig. 4; Table 2) (Shen et al., 1997). The lower part of the clastic sequence, i.e. layers XII–IX, accumulated during a glacial period when seasonal freezing temperatures prevailed in the cave. Frost action was interrupted by humid, probably milder periods where phreatic calcite was deposited in frost cracks, and there was possibly a temporally changing water table. There is a coupled ESR/U-Th date on a mammalian tooth from layer IX giving an age of ca 296 ka (+31/−24) (Jones et al., 2004) (Table 3). Based on the date and the climatic conditions, it is reasonable to assume that this part of the sequence was formed during the interval of glacial MIS 8.

As noted above, layers VII and VI and above mark a change to a different sedimentation pattern characterized by alternating clast to matrix-supported gravel and matrix-rich beds. They are also associated with the densest accumulations of anthropogenic material inside the cave. Layers VII and VI also record three prominent crusts on top of flowstone formations related to bouldery lags. Weathering crusts on the boulders associated with iron–manganese impregnation features in the cemented matrix implies a long exposure and reduced sedimentation of these layers on the floor of the cave (Gillieson, 1996, p. 155). It also appears that these crusts were forming during periods without

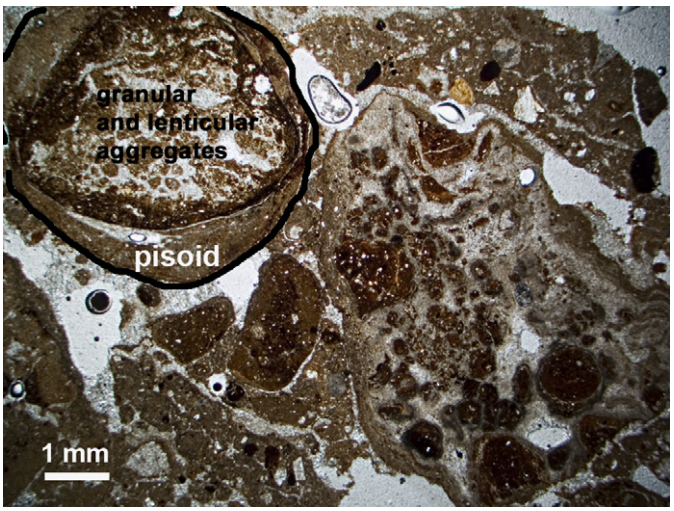

Fig. 9. Microphotograph of complex pisoid structures in layer I. Note that the upper left pisoid has a core of cemented calcite aggregate with lenticular and granular microstructure; PPL.

Fig. 10. Resin-impregnated slab of laminated flowstone of layer I.

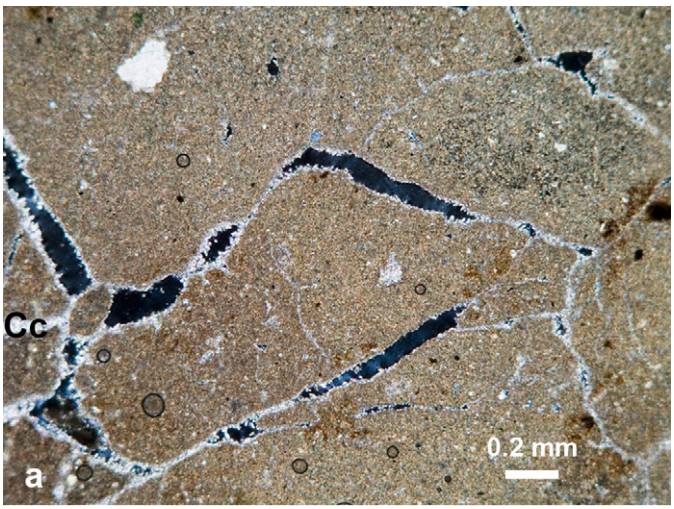

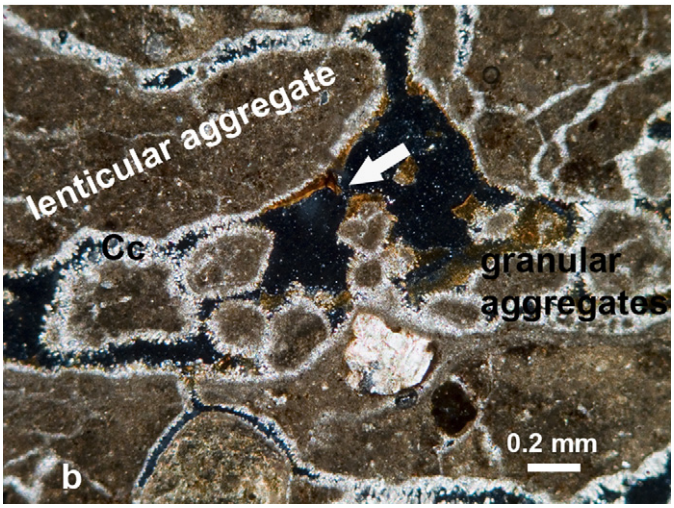

Fig. 11. Microphotographs of (a) homogeneous fine silty calcite with incipient platy microstructure (defined by fissure pattern); layer XXII, plane polarized light (PPL) and (b) lenticular and granular microstructure with grains having rims of bladed calcite (Cc) and dusty clay meniscus coatings (with arrow); layer XXI, crossed polarized light (XPL).

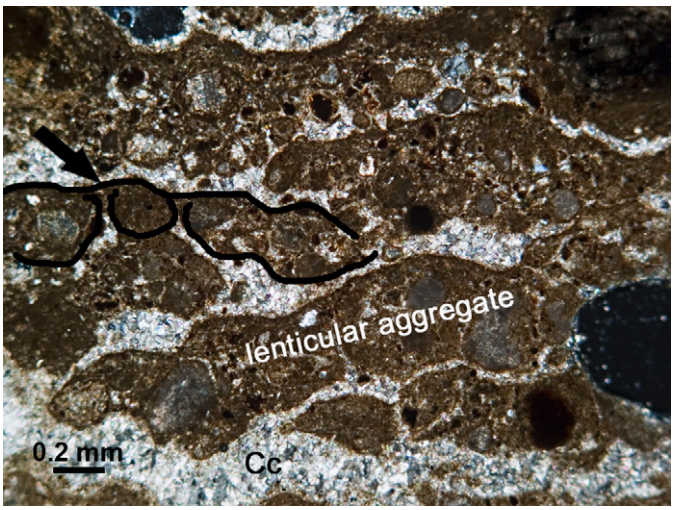

Fig. 12. Lenticular microstructure with link cappings (arrow) and completely filled with sparitic calcite (Cc); layer I, XPL.

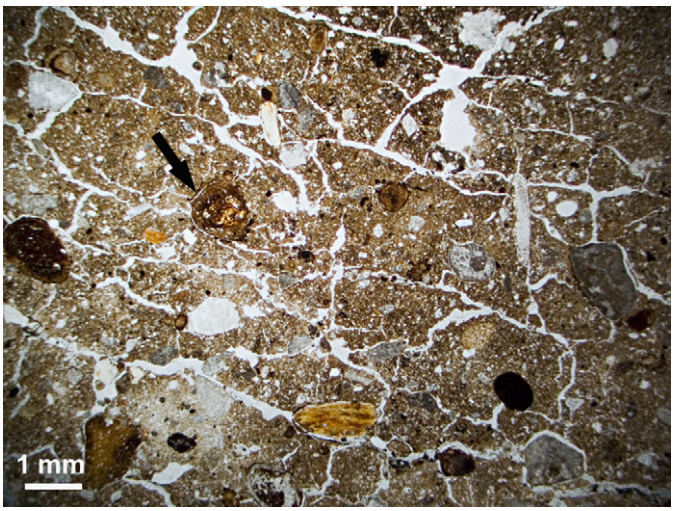

Fig. 13. Microphotograph of incipient platy microstructure (defined by the fissure pattern) and organo-metallic nodules (with arrow); layer II, PPL.

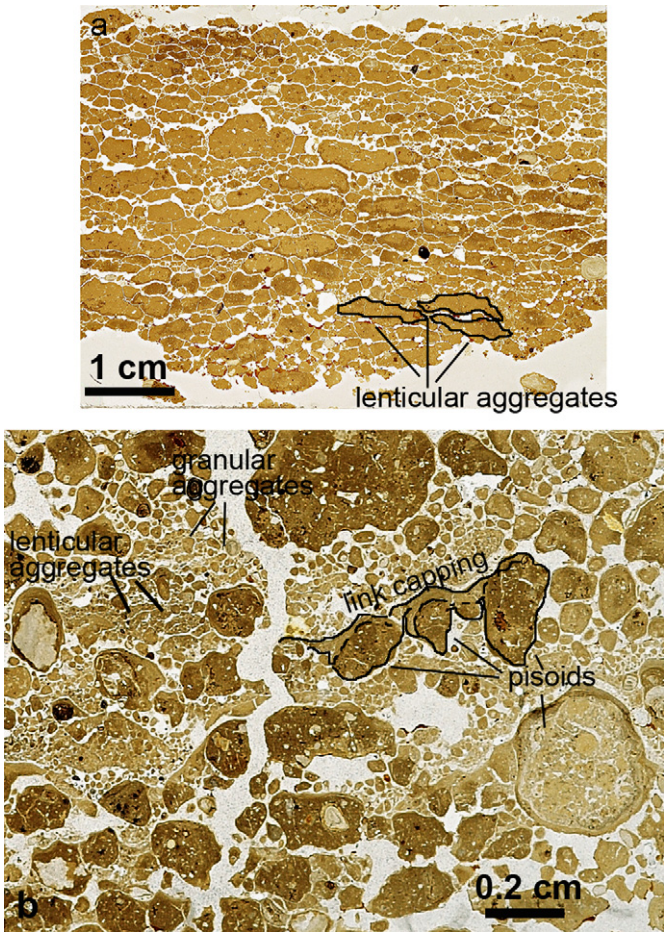

Fig. 14. Photographs of thin sections showing well-developed lenticular microstructure (a) and lenticular to granular microstructure with abundant laminated silty calcite link cappings (b). Note also pisoid structures.

frost action under rather humid and warm climatic conditions when an extensive tree cover would have stabilized the soils above the cave. However, the clastic content of the crusts affected by this weathering process, and possibly even the major part of the flowstones, were forming during previous cold periods, as they are the product of being affected by frost action.

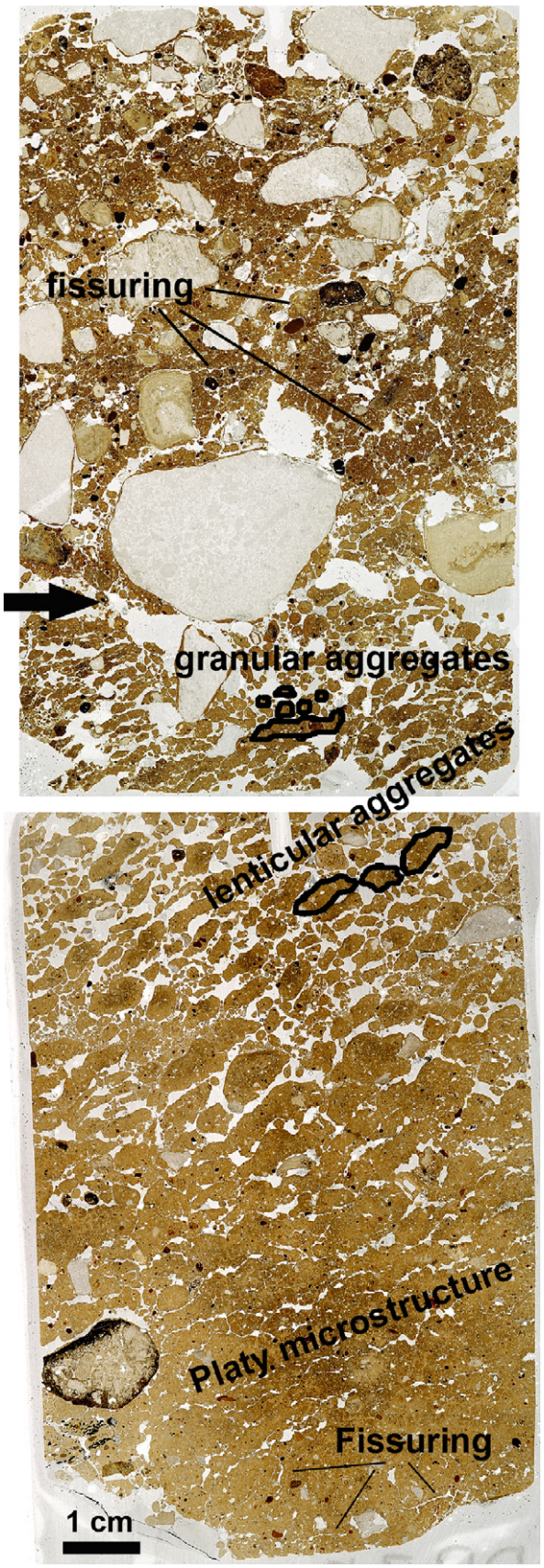

Fig. 15. Sequence of two thin sections. The arrow marks the contact between the underlying loamy layer V and the overlying gravelly layer IV. Note that freeze–thaw features in layer V increase towards the contact with layer IV which shows only fissure microstructure.

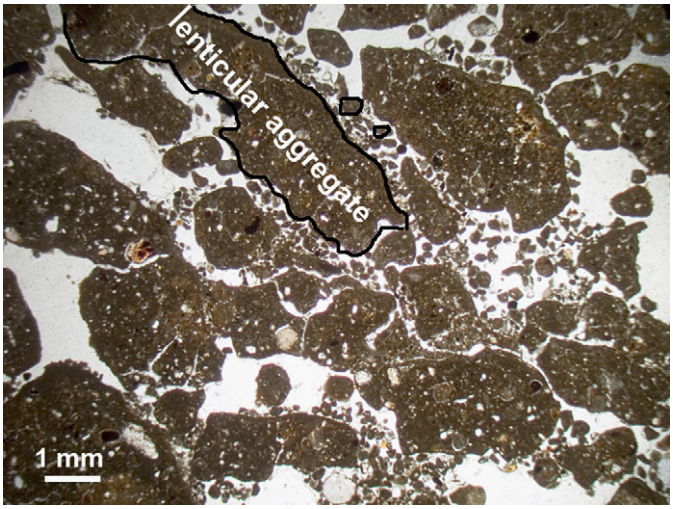

Fig. 16. Microphotograph of lenticular microstructure with voids infilled with loose sorted grains; layer V, PPL.

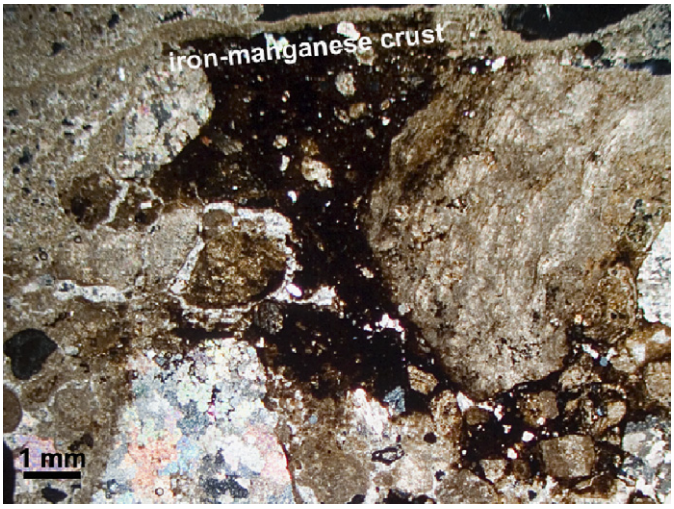

Fig. 18. Microphotograph of iron–manganese crust bridging coarse particles; layer VII, XPL.

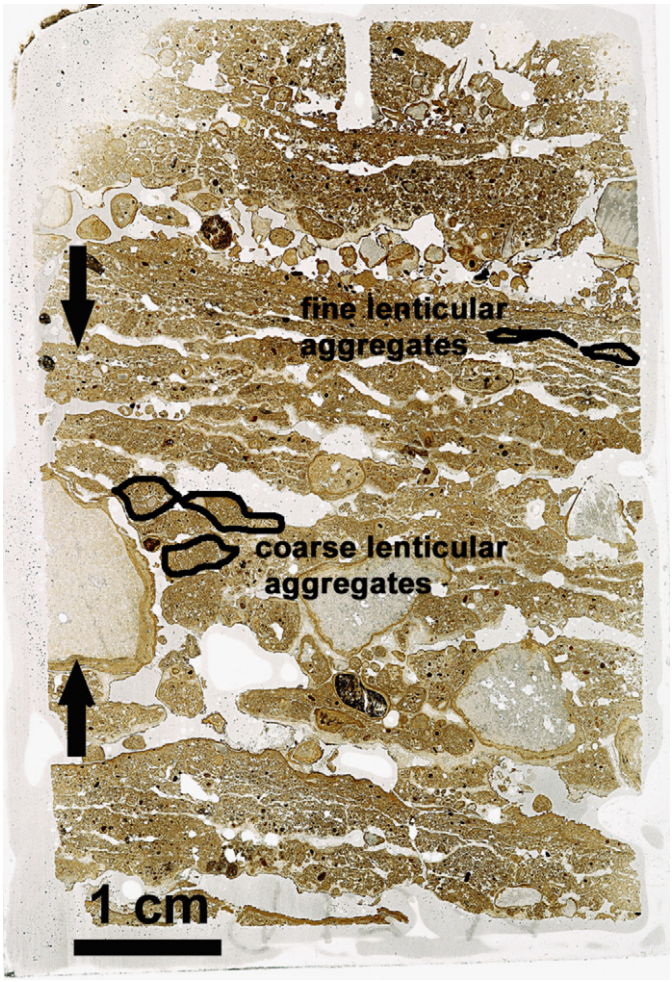

Fig. 17. Photograph of a thin section from layer I showing an increment (between arrows) with decreasing size of ice lensing upwards.

Conventional ESR and coupled ESR/U-series dates on mammalian teeth from these layers assume a minimum age of ca 257 ± 37 ka based on a linear uptake model (Jones et al., 2004) (Table 3). This places them close to the end of MIS 8. However, the mean ESR early uptake model ages for this group are 211 ± 31 ka (Table 3). Unfortunately, given the complex nature of these layers with bouldery facies alternating with hard calcareous crusts in a thin (20–50 cm) sediment slice, it was not possible to determine a better approximation of their exact provenance inside these two complex layers. In addition, a U-Th date from a flowstone sample located 20 m away from the excavation, but linked to one of these crusts on the basis of field stratigraphic correlations (see Figs. 4 and 5), gave a corrected but inconclusive date of ca 260 ka since it was highly contaminated with detrital material (Shen et al., 1997) (Table 2). Nevertheless, given the complex nature of this unit (with beds clearly affected by frost action and others representing hiatuses under milder climatic conditions and containing sediment frequently redeposited), layers VI and VII should correspond to MIS 7 along with potentially redeposited material from MIS 8. Some of the dated teeth that show a marked deviation from the mean value (Table 3) might be also explained in the same way. It is tempting to assume that the three crusts might represent the three warm substages of MIS 7 (e, c and a) (Pisias et al., 1984), but additional data are required before this is substantiated.

Layers V–II show a similar depositional pattern with fluctuating frost intensity. There are thick matrix-rich layers with high organic content that show evidence of freeze–thaw activity, although some layers have only fissuring and incipient coarse platy microstructure. However, sedimentation and frost action were more or less contemporaneous processes throughout the formation of the sequence, and it seems that the pattern is consistent with sedimentation mainly produced under a glacial climate, intensive hill erosion, and fluctuating humidity. It is also evident that some flowstones accompany coarse gravel sheetflow facies. This implies a wetter environment when episodic sediment flows were accompanied by constant dripping and surface water flows. Coupled ESR/U-Th dates on mammalian teeth from these layers suggest a minimum age of 156 ± 17 ka (Jones et al., 2004) (Table 3) placing their formation inside the glacial MIS 6 in accordance with the observed freeze–thaw features. This is in agreement with the two flowstone formations dated in the area to the north of the excavation and correlated with the flowstone formations inside the complex layers III and II close to the north wall (see Figs. 4 and 5). They had corrected ages (due to their contamination with clastic material) of 190 and 160 ka, respectively (Shen et al., 1997) (Table 2).

Table 2
U/Th dating of speleothems from Dadong Cave (after Shen et al., 1997)

Sample	Description	U (ppm)	$^{230}Th/^{232}Th$	$^{234}U/^{238}U$	$^{230}TH/^{234}U$	^{230}Th age (ka)	Corrected age $(^{230}Th/^{232}Th)_0 = 1$	Corrected age $(^{230}Th/^{232}Th)_0 = 2$
9311-6	Layer I	0.07	12.3	1.207 ± 0.031	0.785 ± 0.026	$155^{+13}/_{-11}$	149	142
9509-1	Layer I	0.11	73	1.218 ± 0.021	0.694 ± 0.016	$122^{+6}/_{-5}$		
9509-3	Layers II–III	0.07	18.1	1.134 ± 0.017	0.861 ± 0.017	$198^{+13}/_{-11}$	193	189
9509-4	Layers II–III	0.05	17.2	1.176 ± 0.019	0.814 ± 0.017	$169^{+10}/_{-9}$	165	160
9311-3	Layers VI–VII	0.14	10.1	1.135 ± 0.019	0.960 ± 0.023	$284^{+44}/_{-31}$	274	264
9205-6	Bell canopy	0.07	37.6	1.062 ± 0.022	0.983 ± 0.016	$360^{+189}/_{-64}$		
9209-4	Bell canopy	0.08	21.5	1.088 ± 0.017	0.968 ± 0.024	$308^{+65}/_{-40}$		

In samples with $^{230}Th/^{232}Th$ less than 20 the initial ^{230}Th contribution to the age result is corrected. Age results of samples with $^{230}Th/^{232}Th$ less than 10 are not shown here as they are considered unreliable (Shen et al., 1997). The stratigraphic assignment of the samples is based on field correlations during the present study (see also Fig. 4).

Table 3
ESR and U-series dating results form Dadong Cave (after Jones et al., 2004)

Sample	Layer	EU ESR age (ka)	LU ESR age (ka)	Coupled ESR-$^{230}Th/^{234}U$ age (ka)
Upper group				
PD4C	II–IV	118 ± 14	131 ± 18	
PD6A	II–IV	160 ± 22	182 ± 25	$208^{+23}/_{-19}$
PD3a	II–IV	124 ± 14	166 ± 21	
PD8A	II–IV	144 ± 23	154 ± 26	
PD10A	II–IV	142 ± 15	149 ± 23	
Mean		137 ± 15	156 ± 17	
Lower group				
ESR 26A	VI–VII	159 ± 26	185 ± 31	
ESR 22A	VI–VII	158 ± 20	210 ± 28	
ESR 20A	VI–VII	184 ± 30	219 ± 34	$231^{+32}/_{-26}$
ESR 25A	VI–VII	228 ± 39	274 ± 44	
ESR 24A	VI–VII	233 ± 34	296 ± 42	$294^{+35}/_{-30}$
ESR 24B	VI–VII	296 ± 54	349 ± 58	
PD17A	VI–VII	247 ± 29	301 ± 42	
PD18A	VI–VII	195 ± 21	250 ± 32	
PD16A	VI–VII	199 ± 26	228 ± 17	
Mean		211 ± 31	257 ± 37	
PD15a	IX	214 ± 24	268 ± 36	$296^{+31}/_{-24}$

Stratigraphic assignment to specific layers is based on sample projection onto the profiles during the present study. Nevertheless, sample grouping and mean values are as presented by Jones et al. (2004), except for sample PD15 that is separated from the lower group. Sample PD6A shows a recent uptake or episodic uranium gain and losses. For full discussion of the results see Jones et al. (2004).

Layer I is of special interest because it provides some more detailed information on the conditions prevailing during the formation of thick flowstones in Dadong. This flowstone is one of the unique examples of calcite precipitation under intermittent frost action inside a cave. It actually consists of consecutive reworked clastic calcareous material deposited by low energy sheetflow. One of the actual main sources of the clastic material was the frost action that fragmented the previously deposited moderately cemented sediments. Seasonal alternation of freeze and thaw cycles might explain the unique characteristics of these deposits. At the same time, calcite was precipitating in inter- and intra-aggregate pores. Intraclast precipitation might have been active seasonally during the thawing cycle since pisoids are cemented inside the ice lenses, but interaggregate calcite is not affected by frost action in contrast to what is seen in other layers (e.g. XI, IV and III). It is actually the material that gives the overall flowstone appearance of the deposit. The cementation was followed with dusty clay and silty vadose features. The overall structure of the flowstone is related to glacial humid climatic conditions with some regularly intervening milder conditions.

The uppermost cap of the flowstone was dated with U-Th by Shen et al. (1997) to ca 130 ka (Table 2; Fig. 4). Thus, the main part of the flowstone should correspond to the lower part of MIS 6. A sample from the uppermost preserved 10 cm of the flowstone is not affected by frost action suggesting that flowstone formation continued into the ensuing interglacial but with reduced intensity. This seems to be the case with the stratigraphically lower flowstones and particularly those related to the crusts in layers VI and VII. During interglacials flowstone formation was considerably reduced, probably due to limited water flow inside the cave. However, we do not have information on the other type of speleothem formations like stalagmites and stalactites that are pure dripstones (but see Section 7).

7. Discussion

The clastic sequence of Dadong cave was formed predominantly during glacial periods. Impure flowstones and generally enhanced calcite precipitation in the sediments were recorded at the same time, but probably during wetter and milder periods. Sedimentation rates and flowstone formation were reduced during interglacial times. Today, water dripping and speleothem formation in Dadong is minimal and flowstone formation is actually absent. Although the modern constructions in the front of the entrance do not seem to impede speleothem formation in the interior, the considerable forest clearance and agricultural activities on the hill above the cave might have disturbed the karstic system. In addition, the modern configuration of the cave with a widened entrance, the considerable dimensions of the cave cross-section, and the formation of the pitfall in the back create a strong air current that produces less than ideal humidity conditions for speleothem formation. In any case, although the configuration of the entrance and the back pitfall might have changed through time, the large dimensions of the cave demand enhanced water flow and humidity for flowstones to be formed. Another explanation for the interruption in speleothem formation is the large amount of organic cave sediments formed during warm stages. The surface deposits of Dadong were a source of nitrates for the production of gunpowder in the recent past. Nitrates are formed on the surface of caves by evaporation in warm, relatively dry and well-ventilated conditions. A major source of nitrates is surface rich organic soils (Hill and Forti, 1997, pp. 157–158; Onac, 2005). The deposition of nitrates may be further aided by various nitrogenous bacteria (Culver, 2005). The formation of iron and manganese crusts, observed in layers VI and VII, is also partially attributed to bacterial activity and the breakdown of organic material (Culver, 2005). Hence, we suggest that during warmer interglacials, waters percolating through rich organic densely vegetated soils were entering Dadong where enhanced bacterial activity formed iron–manganese crusts and

nitrate formations. Under these conditions speleothem formation was considerably suppressed.

On the basis of the freeze–thaw features, during glacial periods the mean temperature in Dadong cave through the winter months was probably a few degrees below zero in order for ice to develop and remain inside the sediment. The only available climatic data in the region (Guizhou Province) come from the last part of the penultimate glacial from two caves to the east, the Qixing and Dongge caves (Fig. 1) (Yuan et al., 2004; Zhang et al., 2004). Based on isotopic studies of speleothem formations, Zhang et al. (2004) suggest a minimum temperature range from 0.65 to −1.43 °C during the coldest stage of the penultimate glacial period. Given that the elevations of Qixing and Dongge are lower (1000 and 680 m, respectively) than that of Dadong (1700 m), we expect that the latter would have temperatures a few degrees lower. This is consistent with the present temperature differences between Dadong and the other caves (15.6 and 18.3 °C vs. 14 °C). However, we have to stress that freezing temperatures are frequently recorded in the Dadong sequence and are not restricted to a certain layer that corresponds only to one glacial period. It is important to note that freezing temperatures are apparent during both MIS 6 and 8 in Dadong Cave. At least seven discrete episodes of frost activity are recorded in the sequence representing MIS 6 and three in MIS 8. The latter, however, does not represent the complete time span of this glacial period, as the excavation did not reveal the full development of this part of the sequence. The type of freeze–thaw activity recorded in Dadong, i.e. lenticular and granular microstructures, is related to a long series of alternating freezing and thawing (Van Vliet-Lanoë et al., 1984) and is not the product of a few extreme seasonal climatic excursions. For an area with a subtropical climate at present, this is probably unexpected. In any case, given that the mean temperature of the coldest month today is ca 5 °C, it is certain that a seasonal drop of at least 6–7 °C is expected for long portions of the glacial periods.

Pollen studies from coastal subtropical areas in China suggest a cooler and wetter climate during parts of the last glacial but drier conditions during the Last Glacial Maximum. However, in the western highlands of Yunnan to the south of Dadong Cave, the pollen studies show that rainfall should be higher in the glacial than in the interglacial. A drop in temperature of 4–6 °C is also estimated (Zheng, 2000). Yet contrasting evidence for the distribution of C4 and C3 plants during the late part of the penultimate glacial is recorded from the caves of Qixing and Dongge (Zhang et al., 2004). Qixing Cave (Fig. 1), at the higher elevation than Dongge, records a very high ratio of C3 to C4 plants during part of the glacial, exceeding the value for the interglacial. This should be interpreted as higher precipitation during glacial intervals. Periods with high precipitation in cold stages of the penultimate glacial are also reported from isotopic studies of speleothems from caves in subtropical Guilin, Guangxi Province (Zhang et al., 2006). Even so, the consensus is that during glacial times in the subtropics, the climate was considerably drier due to a weakened summer and a strengthened winter monsoon (Wang et al., 2001; Yuan et al., 2004; for a review see also Wang et al., 2005). Yuan et al. (2004) conducted oxygen isotopic analysis of speleothems formed over the past 160,000 years in Guizhou. Their sample includes Dongge Cave, already discussed above, situated at a slightly more southern latitude (25°17′N) and lower elevation than Dadong (Fig. 1), with a comparable annual temperature (15.6 °C) but higher precipitation (1753 mm). They suggest a considerably drier climate during glacial times. In comparison, the Dadong sedimentary record supports the scenario of high effective precipitation during intervals of the glacial periods that were also characterized by low temperatures and reduced vegetation cover. This contrasts with the other speleothem studies in the area that record enhanced precipitation only during very warm interstadials (Zhang et al., 2004). A possible explanation could be that Dadong, situated at 105 °E longitude at the boundary between the Indian and East Asian monsoons (Wang et al., 2005), belongs to a different precipitation regime than the rest of subtropical southern China where these other sites are located. Modeling experiments have shown that this is also roughly the boundary between areas of contrasting precipitation during different climatic stages (de Noblet et al., 1996). It is also in agreement with the past climatic characteristics of several Chinese regions during wet and dry monsoons in relation to the snow cover in Eurasia (Yang and Xu, 1994). The possibility of a strong monsoon under a glacial climate was also suggested by simulation studies (Masson et al., 2000). Furthermore, Ju et al. (2007) showed that the simulated annual precipitation during the Last Glacial Maximum is higher in western China than present in contrast with eastern China. As Wang et al. (2005) clearly pointed out, monsoon variability is not a direct linear response to global ice volume and thus should not be considered only in the context of glacial–interglacial variability. The Dadong cave sequence provides strong indications of enhanced monsoons under glacial climate with temperatures much lower than today.

The faunal record at Dadong provides additional evidence for the climatic conditions prevailing during the formation of the deposits. The frequent intercalation of flowstones and calcified and non-calcified clastics, with the former building extensive caps on the underlying clastic deposits, assures that artifacts and bones are more or less contemporaneous with the enclosing strata (cf Moriarty et al., 2000). Formation processes of each layer, however, include transport and reworking along distances restricted to their lateral and horizontal extensions. Some crude lateral sorting is evident from a preliminary analysis of the sizes of the bone in each layer although taphonomic surface analysis of the assemblage precludes major post-depositional alteration of the fauna (Schepartz et al., 2003; Bekken et al., 2004). Nevertheless, during interglacials the combination of reduced sedimentation, enhanced bacterial activity, and the associated production of acidic waters (Culver, 2005) would have resulted in the dissolution of bones accumulated on the surface of the cave. Interestingly, there are no indications of enhanced dissolution of the carbonates (limestone clasts, flowstones, etc.). Furthermore, widespread chemical alteration in the form of phosphate mineralization that normally occurs in cave environments and is partly attributed to bone dissolution (Karkanas et al., 2000) is not recorded in any of the Dadong layers. Some smaller bones that accumulated during the formation of the weathering crusts might have dissolved away, but the evidence does not support dissolution to any extent that would alter the faunal composition. Thus, fauna in Dadong can be evaluated in the light of the environmental conditions responsible for the accumulation of each layer.

A mixed woodland environment with two or three habitats including bamboo forests and open rocky areas with abundant grasses is suggested by the fauna composition. One of the striking characteristics of the Dadong fauna is the consistency of taxonomic representation over time (Bekken et al., 2004). Given the environmental interpretation of the depositional sequence, with the vast majority of the material being accumulated during glacial times, this consistency is not entirely unexpected. Most of the abundant Dadong species are highly adaptable forms with fairly broad environmental ranges. However, indications of heavy or closed canopy forests are not encountered in Dadong, unlike the cave site of Tongzi in northern Guizhou (Olsen and Miller-Antonio, 1992). The fauna of this site seems to be derived from a layer dated to the interglacial MIS 7.

It is also important to note that the majority of the taxa found in Dadong are not habitual cave dwellers. Carnivores were only present in small numbers and indications of rodent and carnivore

modifications of the fauna assemblage are not an important taphonomic feature (Bekken et al., 2004). Hominin produced bone modifications in the form of cutmarks, percussive damage and burning are relatively scarce, but stone tools are found throughout the deposits. In conclusion, combining all the evidence above, it is not unreasonable to assume that hominins are the primary agent of faunal accumulation in Dadong and therefore may have been responsible for the relative consistency of the assemblage over time. But it also appears that hominins were probably not present during interglacials periods, and that carnivore use of the cave did not increase during their absences, as has been documented for many cave faunas (cf Stiner, 1991). One explanation might be that the denser subtropical forests of the interglacial could have resulted in lower prey densities of the large animals such as *Stegodon*, *Rhinoceros* and many large bovids and cervids that are frequently found in the Dadong depositional sequence. Alternatively, the hominin use of the cave for shelter and warmth might not have been necessary during the warmer interglacials.

8. Conclusion

The frequent alternation of flowstone formation, cementation, clastic deposition, and frost activity in the depositional sequence of Dadong Cave is used to reconstruct the environmental conditions prevailing during the later Middle Pleistocene on the Guizhou Plateau. The sedimentary sequence was deposited mainly during the glacial intervals of MIS 8 and 6.

Clastic deposits were entering the cave in the form of intermittent cohesive debris flows and sheetflows. The sources of the clastic sediment were soils and sediment in the vicinity of the cave, transported under a cold and relatively dry climate when vegetation cover was reduced. Interlayered impure flowstones were forming during wetter phases but still under glacial conditions. The frequent occurrence of cycles of well-developed freeze–thaw features affecting both the clastic parts of the sequence and the flowstones as they were deposited suggests unexpectedly low seasonally freezing temperatures. At the same time, remains of hominin activities in the form of faunal remains and lithic artifacts were accumulating on the surface of the fan-like sedimentary sequence and redistributed laterally along the different depositional facies. During the intervening interglacial of MIS 7 and possibly MIS 5, clastic deposition was minimal and sedimentation was restricted to thin flowstone caps and weathering manganese–iron crusts. Hominins were probably not present during interglacials periods—perhaps due to lower prey densities of the large animals in the denser subtropical forests of the interglacial or a diminished need for the sheltering benefits the cave offered. Consequently, a relative consistency of the faunal assemblage over time is observed, with temperature-resistant forms constituting the bulk of the taxa. Most notably, the primates and suids that are typically associated with subtropical faunas are only minimally represented.

Analysis of the Dadong sequence suggests that precipitation was much higher during glacial intervals than interglacials under a predominantly cold climate. Other paleoclimatic studies, based on pollen or simulation studies, point toward the same conclusion, although the current state of our knowledge of climatic conditions in southern China from fauna and speleothems indicates considerable diversity relating to elevation and geographical position. Dadong Cave may present its distinctive signature of very cold and wet climatic conditions during glacials in the subtropics of East Asia because it is situated precisely in the area where the Indian and East Asian monsoon effects converge.

Acknowledgments

The authors would like to thank the other members of the Panxian Dadong Collaborative Project for their input toward the field research that this analysis is based upon: Kanai Paraso, Liu Jun, Si Xinqiang, Deborah Bekken, Hou Yamei and the fieldworkers from Dadong. Our research was supported by the National Geographic Society (2005–2006), The Henry Luce Foundation (1998–2001), NSF (1997), the Wenner-Gren Foundation (1996) and the LSB Leakey Foundation (1996).

References

Ayliffe, L.K., Marianelli, P.C., Moriarty, K.C., Wells, R.T., McCulloch, M.T., Mortimer, G.E., Hellstrom, J.C., 1998. 500 ka precipitation record from southeastern Australia: evidence for interglacial aridity. Geology 26, 147–150.

Baker, A., Smart, P.L., Ford, D.C., 1993. North-west European palaeoclimate as indicated by growth frequency variations of secondary calcite deposits. Palaeogeography, Palaeoclimatology, Palaeoecology 100, 291–300.

Bar-Matthews, M., Ayalon, A., Gilmour, M., Matthews, A., Hawkesworth, C.J., 2003. Sea-land oxygen isotopic relationships from planktonic foraminifera and speleothems in the Eastern Mediterranean region and their implication for paleorainfall during interglacial intervals. Geochimica et Cosmochimica Acta 67, 3181–3199.

Bekken, D., Schepartz, L.A., Miller-Antonio, S., Hou, Y., Huang, W., 2004. Taxonomic abundance at Panxian Dadong, a Middle Pleistocene cave in South China. Asian Perspectives 43, 333–359.

Blikra, R.H., Nemec, W., 1998. Postglacial colluvium in western Norway: depositional processes, facies and palaeoclimatic record. Sedimentology 45, 909–959.

Bullock, P., Fedorroff, N., Jongerius, A., Stoops, G.I., Tursina, T., 1985. Handbook for Soil Thin Section Description. Waine Research Publishers, Wolverhampton.

Courty, M.A., Vallverdu, J., 2001. The microstratigraphic record of abrupt climate change in cave sediments of the western Mediterranean. Geoarchaeology 16, 467–500.

Courty, M.A., Goldberg, P., Macphail, R., 1989. Soils and Micromorphology in Archaeology. Cambridge University Press, Cambridge.

Culver, D.S., 2005. Microbes. In: Culver, D.C., White, W.B. (Eds.), Encyclopedia of Caves. Elsevier Academic Press, Burlington, pp. 369–371.

de Noblet, N., Braconnot, P., Joussaume, S., Masson, V., 1996. Sensitivity of simulated Asian and African summer monsoons to orbitally induced variations in insolation 126, 115 and 6 kBP. Climate Dynamics 12, 589–603.

Farrand, W.R., 2001. Sediments and stratigraphy in rockshelters and caves: a personal perspective on principles and pragmatics. Geoarchaeology 16, 537–557.

Gillieson, D., 1996. Caves: Processes, Development, Management. Blackwell Publishers, Oxford.

Goldberg, P., Sherwood, S.C., 2006. Deciphering human prehistory through the geoarchaeological study of cave sediments. Evolutionary Anthropology 15, 20–36.

Gremaschi, M., Van Vliet-Lanoë, B., 1990. Traces of frost activity and ice segregation in Pleistocene loess deposits and till of northwestern Italy: deep seasonal freezing or permafrost? Quaternary International 5, 39–48.

Hill, C., Forti, P., 1997. Cave Minerals of the World, second ed. National Speleological Society, Huntsville.

Jones, H.L., Rink, J.W., Schepartz, L.A., Miller-Antonio, S., Huang, W., Hou, Y., Wang, W., 2004. Coupled electron spin resonance (ESR)/uranium-series dating of mammalian tooth enamel at Panxian Dadong, Guizhou Province, China. Journal of Archaeological Science 31, 965–977.

Ju, L., Wang, H., Jiang, D., 2007. Simulation of the Last Glacial Maximum climate over East Asia with a regional climate model nested in a general circulation model. Palaeogeography, Palaeoclimatology, Palaeoecology 248, 376–390.

Karkanas, P., 2001. Site formation processes in Theopetra cave: a record of climatic change during the Late Pleistocene and early Holocene in Thessaly, Greece. Geoarchaeology 16, 373–399.

Karkanas, P., Bar-Yosef, O., Goldberg, P., Weiner, S., 2000. Diagenesis in prehistoric caves: the use of minerals that form in situ to assess the completeness of the archaeological record. Journal of Archaeological Science 27, 915–929.

Knapp, E.P., Terry, D.O., Harbor, D.J., Thren, R.C., 2004. Reading Virginia's paleoclimate from geochemistry and sedimentology of clastic cave sediments. In: Sasowsky, I.D., Mylroie, J. (Eds.), Studies of Cave Sediments: Physical and Chemical Records of Paleoclimate. Kluwer Academic/Plenum Publishers, New York, pp. 95–106.

Kukla, G., 1987. Loess stratigraphy in central China. Quaternary Science Reviews 58, 191–219.

Lister, G.S., Kelts, K.R., Chen, K.Z., Yu, J.Q., Niessen, F., 1991. Lake Qinghai, China: closed-basin lake levels and the oxygen isotope record for ostracoda since the latest Pleistocene. Palaeogeography, Palaeoclimatology, Palaeoecology 84, 141–162.

Masson, V., Braconnot, P., Jouzel, J., de Noblet, N., 2000. Simulation of intense monsoons under glacial conditions. Geophysical Research Letters 27, 1747–1750.

Miller-Antonio, S., Schepartz, L.A., Bekken, D., 2000. Raw material selection and evidence for rhinoceros tooth tools at Dadong Cave, southern China. Antiquity 74, 372–379.
Miller-Antonio, S., Schepartz, L.A., Karkanas, P., Hou, Y., Huang, W., Bekken, D., 2004. Lithic raw material use at the Late Middle Pleistocene site of Panxian Dadong. Asian Perspectives 43, 314–332.
Moriarty, K.C., McCulloch, M.T., Wells, R.T., McDowell, M.C., 2000. Mid-Pleistocene cave fills, megafauna remains and climate change at Naracoorte, South Australia: towards a predictive model using U-Th dating speleothems. Palaeogeography, Palaeoclimatology, Palaeoecology 159, 113–143.
Nickling, W.G., 1994. Aeolian sediment transport and deposition. In: Pye, K. (Ed.), Sediment Transport and Depositional Processes. Blackwell Scientific Publications, Oxford, pp. 293–350.
Olsen, J.W., Miller-Antonio, S., 1992. The Palaeolithic in southern China. Asian Perspectives 21, 129–160.
Onac, B.P., 2005. Minerals. In: Culver, D.C., White, W.B. (Eds.), Encyclopedia of Caves. Elsevier Academic Press, Burlington, pp. 371–378.
Pisias, N.G., Martinson, D.G., Moore, T.C., Shackleton, N.J., Prell, W., Hays, J., Boden, G., 1984. High resolution stratigraphic correlation of benthic oxygen isotopic records spanning the last 300,000 years. Marine Geology 56, 119–136.
Schepartz, L.A., Bekken, D., Miller-Antonio, S., Paraso, C.K., Karkanas, P., 2003. Faunal approaches to site formation processes at Panxian Dadong. In: Shen, C., Keates, S. (Eds.), Current Research in Chinese Pleistocene Archaeology. BAR International Series.
Scholle, P.A., Ulmer-Scholle, D.S., 2003. A Color Guide to the Petrography of Carbonate Rocks: Grains, Textures, Porosity, Diagenesis. AAPG Memoir 77, Tulsa.
Shen, G., Liu, J., Jin, L., 1997. Preliminary results on U-series dating of Panxian Dadong in Guizhou province, S–W China. Acta Anthropologica Sinica 16, 221–230 (Chinese with English abstract).
Springer, G.S., 2005. Clastic sediments in caves. In: Culver, D.C., White, W.B. (Eds.), Encyclopedia of Caves. Elsevier Academic Press, Burlington, pp. 102–108.
Stiner, M.C., 1991. The faunal remains from Grotta Guattari: a taphonomic perspective. Current Anthropology 32, 103–117.
Stoops, G., 2003. Guidelines for Analysis and Description of Soil and Regolith Thin Sections. Soil Science Society of America, Madison, WI.
Thompson, L.G., Yao, T., Davis, M.E., Henderson, K.A., Mosley-Thompson, E., Lin, P.N., Beer, J., Synal, H.A., Cole-Dai, J., Bolzan, J.F., 1997. Tropical climate instability: The Last Glacial Cycle from Qinghai-Tibetan ice core. Science 276, 1821–1825.
Van Vliet-Lanoë, B., Coutard, J.P., Pissard, A., 1984. Structures caused by repeated freezing and thawing in various loamy sediments: a comparison of active, fossil and experimental data. Earth Surface Processes and Landforms 9, 553–565.
Wang, Y.J., Cheng, H., Edwards, R.L., An, Z.S., Wu, J.Y., Shen, C.C., Dorale, J.A., 2001. A high-resolution absolute-dated Late Pleistocene monsoon record from Hulu Cave, China. Science 294, 2345–2348.
Wang, W., Liu, J., Hou, Y., Si, X., Huang, W., Schepartz, L.A., Miller-Antonio, S., 2004. Panxian Dadong, South China: establishing a record of Middle Pleistocene climatic changes. Asian Perspectives 43, 302–313.
Wang, P., Clemens, S., Beaufort, L., Braconnot, P., Ganssen, G., Jian, Z., Kershaw, S., Sarnthein, M., 2005. Evolution and variability of the Asian monsoon system: state of the art and outstanding issues. Quaternary Science Reviews 24, 595–629.
Weiner, S., Goldberg, P., Bar-Yosef, O., 1993. Bone preservation in Kebara Cave, Israel using on-site Fourier Transform Infrared spectrometry. Journal of Archaeological Science 20, 613–627.
Woodward, J.C., Goldberg, P., 2001. The sedimentary records in Mediterranean rockshelters and caves: archives of environmental change. Geoarchaeology 16, 327–354.
Xiong, K., Liu, J., 1997. Development and evolution of the Panxian Dadong cave. Acta Anthropologica Sinica 16, 239–246 (Chinese with English abstract).
Yang, S., Xu, L., 1994. Linkage between Eurasian winter snow cover and regional Chinese summer rainfall. International Journal of Climatology 14, 739–750.
Yuan, D., Cheng, H., Edwards, R.L., Dykoski, C.A., Kelly, M.G., Zhang, M., Qing, J., Lin, Y., Wang, Y., Wu, J.Y., Dorale, J.D., An, Z.S., Cai, Y., 2004. Timing, duration, and transitions of the Last Interglacial Asian monsoon. Science 304, 575–578.
Zhang, M., Yuan, D., Lin, Y., Cheng, H., Qin, J., Zhang, H., 2004. The record of paleoclimatic change from stalagmites and the determination of termination II in the south of Guizhou Province, China. Science in China Series D Earth Sciences 47, 1–12.
Zhang, M., Hai, C., DaoXian, Y., Z., X., Yushi, L., Jiaming, Q., Edwards, R.L., 2006. Carbon and oxygen isotope records and paleoclimate reconstruction (140–250 ka B.P.) from a stalagmite of Shuinan Cave, Guilin, China. Environmental Geology 49, 752–764.
Zheng, Z., 2000. Vegetation and climate since the Late Pleistocene in southern China. Journal of Geosciences in China 2, 7–20.
Zheng, B., Xu, Q., Shen, Y., 2002. The relationship between climate change and Quaternary glacial cycles on the Qinghai-Tibetan Plateau: review and speculation. Quaternary International 97/98, 93–101.
Zhu, X., Zhang, M., Lin, Y., Qin, J., Yang, Y., 2006. Carbon isotopic records from stalagmites and the signification of paleo-ecological environment in the area of Guangxi-Guizhou, China. Environmental Geology 51, 267–273.